Solvation Structure and Rotational Dynamics of LiH in ^{4}He Clusters†

Robert E. Zillich*,‡,§ and K. Birgitta Whaley||

Fraunhofer ITWM, 67663 Kaiserslautern, Germany, and Institut für Theoretische Physik, Johannes Kepler Universität, A-4040 Linz, Austria, and Department of Chemistry and Pitzer Center for Theoretical Chemistry, University of California, Berkeley, California 94720

Received: February 20, 2007; In Final Form: May 8, 2007

We present results of path integral Monte Carlo simulations of LiH solvated in superfluid ^{4}He clusters of size up to $N = 100$. Despite the light mass of LiH and the strongly anisotropic LiH−He potential with a large repulsion at the hydrogen end, LiH is solvated inside the cluster for sufficiently large N. Using path integral correlation function analysis, we have determined the dipole ($J = 1$) rotational excitations of the cluster and a corresponding effective rotational constant B_{eff} of the solvated LiH. We predict that B_{eff} is greatly reduced with respect to the gas-phase rotational constant B, to a value of only about 6% of B. This exceptionally large reduction of the rotational constant is due to the highly anisotropic ^{4}He solvation structure around LiH. It does not follow the previously established trend of a relatively small B reduction for light molecules, showing the strongest reduction of all molecules in ^{4}He to date. Comparison of the calculated rotational spectra of LiH in helium obeying Bose and Boltzmann statistics, respectively, demonstrates that the Bose statistics of helium is an essential requirement for obtaining well-defined molecule rotational spectra in helium-4.

I. Introduction

Since the discovery that molecular spectra have narrow lines and retain their symmetry in a superfluid helium matrix, the dynamics of many molecules from the smallest diatoms to large organic molecules have been investigated experimentally and theoretically, by respectively recording or predicting rotational, vibrational, and electronic spectra. The rotational structure of spectra is particularly relevant for understanding the coupling between solute and quantum solvent, because rotational energies of many molecules lie in an energy range compatible with the elementary excitations of ^{4}He, i.e., the phonon−roton spectrum. Much understanding of superfluidity on the microscopic scale has indeed been gained from the study of rotational spectra in ^{4}He. It is found that generally molecules have the same symmetry in helium as in the gas phase but that the effective moments of inertia are increased, i.e., the effective rotational constants are reduced, by varying amounts. Usually a small relative reduction is found for light molecules (gas-phase rotational constant $B \gtrsim 1$ K), while a reduction to about one-third of the gas-phase value is found for heavier molecules ($B \lesssim 1$ K). Reference 1 contains a recent list summarizing the effective rotational constants of a number of molecules that have been experimentally studied in helium droplets. The model of adiabatic following of the normal ^{4}He fraction in the two-fluid model[2,3] can reproduce the latter case of a heavier molecule quite well. For light molecules, however, adiabatic following cannot account for the experimental observations.[4] Instead, we have shown that for fast rotors it is the coupling to collective excitations of the ^{4}He droplets that reduces the effective rotational constant.[5−7]

LiH is a very light (only twice the mass of ^{4}He) and fast ($B = 10.81$ K[8]) linear rotor. However, unlike other light molecules for which the interaction potential with helium is quite isotropic, the LiH−He potential is extremely *anisotropic*.[9] The potential averaged over the vibrational ground state[10] is shown in Figure 1 where it is evident that it also has a large repulsive bubble at the H end of the molecule. This raises two questions: (i) is LiH solvated inside a ^{4}He droplet or does it sit on the surface like H?[11] (ii) Is the effective rotational constant only slightly reduced as for fast rotors such as HCN,[12,13] HCCH,[14] and HF,[15] or is it strongly reduced as observed for heavier molecules such as OCS[16] and N_2O,[17] which interact with the solvating helium via a strongly anisotropic potential? We show in this work that

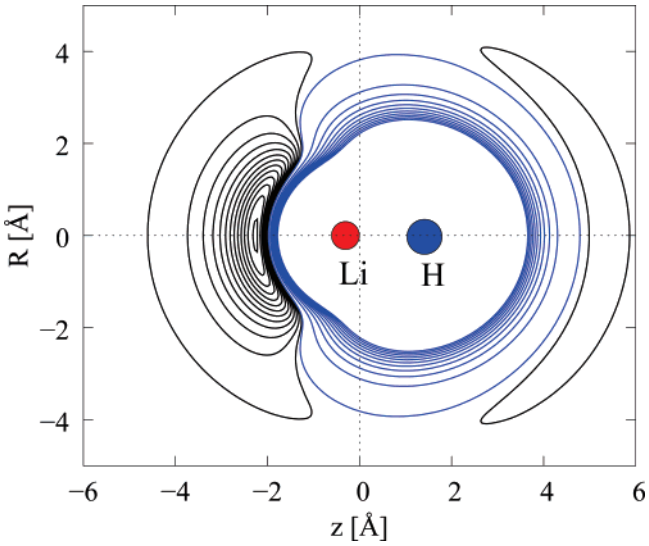

Figure 1. LiH−He interaction potential[10] shown as a contour plot, displayed as a function of the He position (R, z) with respect to LiH, averaged over the vibrational ground state of LiH. z is the distance from the center of mass of LiH (located at the origin) along the molecular axis and R is the radial cylindrical distance from the axis. The equilibrium distance between Li and H is 1.5949 Å, and the circles indicate the atomic positions of Li and H in the classical ground state. Black contours are at − 10, − 30, − 50, ..., K and blue contours at 0, 100, 200, ..., K.

* To whom correspondence should be addressed at the Johannes Kepler Universität.
† Part of the "Roger E. Miller Memorial Issue".
‡ Fraunhofer ITWM, 67663 Kaiserslautern, Germany,
§ Institut für Theoretische Physik, Johannes Kepler Universität.
|| Department of Chemistry and Pitzer Center for Theoretical Chemistry, University of California, Berkeley.

10.1021/jp0714419 CCC: $37.00
Published on Web 07/14/2007

the answer to question i is "inside", while the answer to question ii is that B_{eff} is reduced to a remarkably small fraction of the gas-phase rotational constant B. Hence, LiH lies completely outside the range of typical relative reductions B_{eff}/B that is summarized, e.g., in Figure 13 of ref 18 or in Figure 7 of ref 19.

We now briefly discuss the LiH−He interaction, which we take here from ref 10. This interaction potential was constructed by averaging a three-dimensional *ab initio* potential energy surface over the ground vibrational state of LiH. This vibrationally averaged potential is shown in Figure 1, with the locations of the Li and H atoms in the classical ground state shown for reference. Figure 1 shows that on the Li side, He is strongly attracted to the molecule, while on the H side, He is mostly repelled (there is a secondary minimum, but it is very shallow). This results in a very steep but narrow potential well on the Li side, which constitutes the global minimum. This behavior is qualitatively similar to that exhibited by the combined solute-He interaction of complexes such as HCN−Na in helium droplets, where the bubble due to the Na−He repulsion is even bigger.[20] If we consider a growth sequence from the LiH−^{4}He dimer to LiH interacting with large helium droplets, we expect (and will confirm later) that the first few He atoms will preferably cluster around the global potential minimum. However, as N increases, two scenarios are conceivable. The first is that additional He atoms will go first to the Li side, while the repulsive H side will stay partly "dry" , and then, as the limit of large droplets is approached, LiH will eventually float on the droplet surface, like a beachball (H side) with a plumb weight attached to one side (Li side). The second scenario is that additional He atoms will eventually cover the whole LiH molecule so that in a large droplet, LiH is solvated in the interior.

Considering the interaction potential alone cannot answer this question. For highly quantum particles like ^{4}He and LiH, much depends also on the respective masses and the rotational constant of LiH, and neither scenario can be ruled out without actually solving the Schrödinger equation. Even for the dimer LiH−^{4}He, two extreme situations are possible and cannot be distinguished without explicit calculation. Specifically, either ^{4}He is so strongly bound in the global minimum that the LiH−He dimer is effectively a molecule rather than a van der Waals complex. In this case the potential wins over the (translational and rotational) zero-point motion of ^{4}He and LiH, effectively localizing the helium atom. Alternatively, if the zero-point motion wins over the potential, then ^{4}He will be delocalized and the ^{4}He distribution with respect to the LiH orientation will spread around the LiH molecule. (More exotic, nonclassical structures are also possible, e.g., for Cl_2He.[21]) In section II, we will first present results of quantum calculations of the LiH−^{4}He dimer to answer where on the scale between those two extremes the dimer is situated. Then we will proceed to the more interesting case of larger clusters. In section III, the main results of this work are presented, namely the rotational excitation energies of LiH in ^{4}He clusters ranging from $N = 1$ to $N = 40$. In section IV, we examine the essential role played by Bose statistics, and consequently by superfluidity, for molecular spectra in ^{4}He, with a comparison of the LiH dynamics in calculations made with and without Bose statistics of helium included ("Bose" and "Boltzmann" helium, respectively). Section V concludes.

II. Ground State: Energetics and Structure

For all calculations presented here we use the path integral Monte Carlo (PIMC) technique.[22] Its application to molecular rotations was presented in detail in Ref. 23. As described there, we employ the pair density approach[22] for the (isotropic) He−He interaction, and the primitive appoximation for the (anisotropic) LiH−He interaction. Because of the very steep potential gradient of the LiH−He interaction, we have to be careful with the time step bias, which is proportional to $|\nabla V|^2$.[24] The energy and density distributions associated with atoms in the potential well are most susceptible to time step bias. We start our investigation of the bias with the LiH−^{4}He dimer.

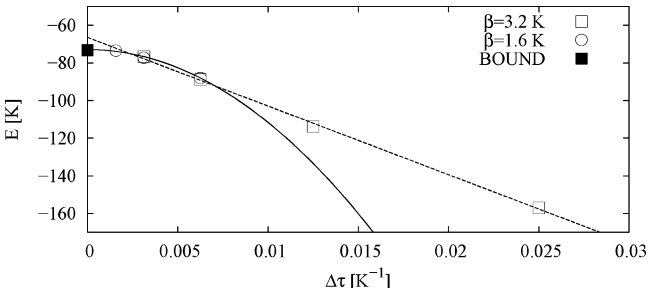

Figure 2. LiH−^{4}He dimer ground state energy E_0 plotted as a function of PIMC time step $\Delta\tau$ and compared with the exact ground energy obtained from BOUND.[25] Open boxes correspond to simulations at $T = 0.3125$ K ($\beta = 3.2$ K^{-1}), open circles to simulations at $T = 0.625$ K ($\beta = 1.6$ K^{-1}). Extrapolation to zero time step is made with a quadratic fit $a + b\Delta\tau^2$ (full line). The dashed line is a linear fit to all data points.

Figure 2 shows the dimer equilibrium energy E_0 (which, at such low T, is the ground state energy, as it will be referred to from now on) for PIMC time step values $\Delta\tau$ = 1/40; 1/80; 1/160; 1/320; 1/640 K^{-1}. Clearly, E_0 exhibits a very strong $\Delta\tau$ bias. Thus, for the largest time step $\Delta\tau$ = 1/40 K^{-1}, which is usually sufficient for pure ^{4}He when the pair density approach is used,[22] E_0 is off by a factor of 2. The time step bias should be proportional to $\Delta\tau^2$ for the primitive approximation to the density matrix. In fact, the strong bias results in a linear $\Delta\tau$ dependence for most of the $\Delta\tau$ range in Figure 2, and the correct asymptotic quadratic $\Delta\tau$ dependence is reached only for the smallest $\Delta\tau$ value. Nevertheless, a quadratic fit through the three smallest $\Delta\tau$ values reproduced (within the error bar) the exact ground state energy $E_0 = -73.3$ K that was obtained independently with the close-coupling program BOUND.[25] The temperature was set to $T = 0.3125$ K, corresponding to $\beta \equiv 1/k_B T = 3.2$ K^{-1} for most of the results presented here and has a negligible effect on E_0, with simulations at $T = 0.625$ ($\beta = 1.6$ K^{-1}) giving identical results (see Figure 2).

In order to address the question of the solvation structure of LiH in ^{4}He, we need to look at both ^{4}He and LiH densities. An important quantity for the understanding of the local quantum solvation environment is the molecule-solvent pair density ρ *i.e.* the helium density in the molecular frame. Let (x,y,z) denote the ^{4}He position with respect to the center of mass of LiH, with the z -axis along the molecule axis, and $R = \sqrt{x^2+y^2}$ is the distance from the molecular axis. Since the interaction potential and hence the helium density has cylindrical symmetry about the molecule axis, the helium density is a function of R and z, $\rho = \rho(R, z)$. Just as for the ground state energy E_0, there is a severe time step bias on the densities. Figure 3 shows the helium density $\rho(R, z)$ for PIMC time steps $\Delta\tau$ = 1/40;1/80;1/160;1/320 K^{-1}. For the largest time step $\Delta\tau$ = 1/40 K, the peak density is more than twice as large as the corresponding density obtained at the smallest value of $\Delta\tau$.

Figure 4 shows the ground state energy $E_0(N)$ for larger clusters $N > 1$ and various time step values $\Delta\tau$. We observe that the N dependence of the ground state energy $E_0(N)$ is almost linear, which implies an almost constant chemical potential

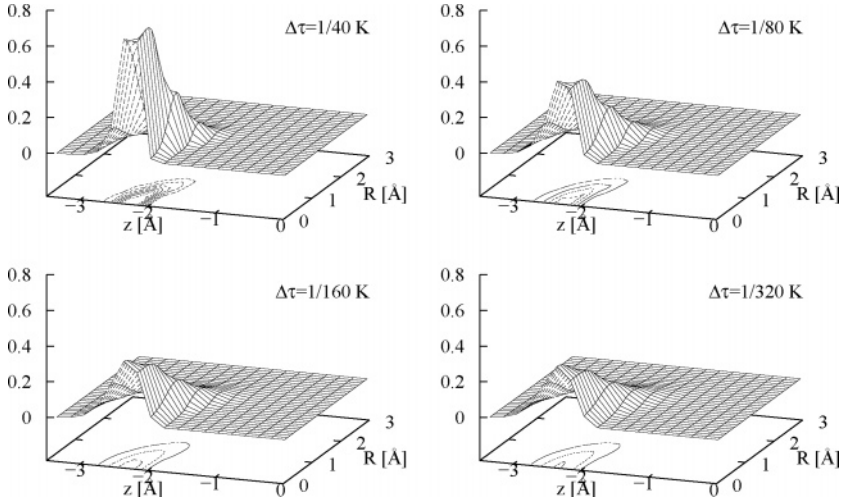

Figure 3. He density relative to the solute LiH is shown for the LiH−He dimer in units of Å^{-3}, as a function of R and z (see Figure 1 for definition of R and z). Densities for calculations with four different values of time step $\Delta\tau$ are compared.

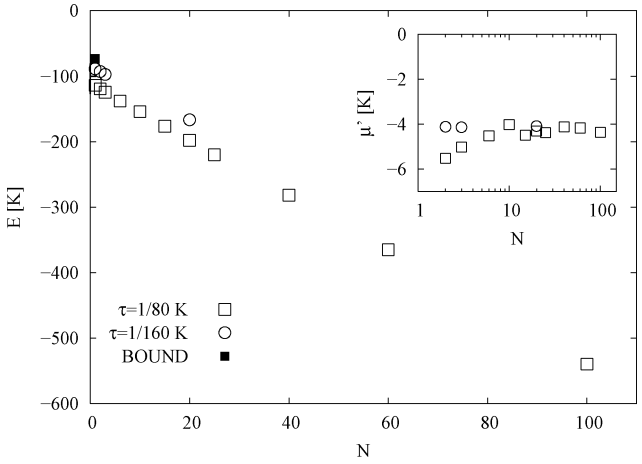

Figure 4. LiH−^{4}He $_N$ ground state energy plotted as a function of cluster size N. The filled square is the exact ground energy for $N = 1$ obtained from BOUND.[25] Open squares correspond to $\Delta\tau = 1/80$ K^{-1}, open circles to $\Delta\tau = 1/160$ K^{-1}. The inset shows the average chemical potential $\mu'(N)$, $N > 1$ (see text for definition). $T = 0.312$K for all simulations here.

$\mu(N) = E_0(N) - E_0(N-1)$ for $N > 1$. In the absence of calculations for every possible size, we can compute the average of the size dependent chemical potential $\mu(N)$ between different sizes $N = N_1 + 1$ and $N = N_2$ from $\mu' = (E_0(N_2) - E_0(N_1))/(N_2 - N_1)$. This is shown as a function of N_2 for $\Delta\tau = 1/80$ K^{-1} in the inset of Figure 4, We see that for $N > 1$, the average quantity $\mu'(N)$ is almost constant, having a value of around -4 K, and is of considerably smaller magnitude than the value of the chemical potential for the $N = 1$ dimer, for which $\mu'(1) = E_0 = -73.3$ K (using the BOUND energy). The time step bias stems largely from the steep global minimum region of the potential, which can accommodate only very few He atoms. Therefore, the time step bias grows slowly beyond $N = 1$. For $N = 1$, the difference in E_0 between $\Delta\tau = 1/80$ K^{-1} and $\Delta\tau = 1/160$ K^{-1} is 25.1 K, while for $N = 20$ the corresponding difference has only increased to 31.6 K.

In Figure 5, we show the ^{4}He$_N$ density $\rho(R,z)$ obtained with a time step $\Delta\tau = 1/80$ K^{-1}, for several sizes between $N = 1$ and $N = 100$. The most marked feature of the helium solvation is its strong anisotropy in the angular direction. Compared to heavier molecules such as OCS, the layering in the radial direction is less marked, except for the region around the global potential minimum. Because of the strong asymmetry of the interaction potential (Figure 1), the first few ^{4}He atoms tend to cluster in and around the global minimum on the Li side of LiH. (See Figure 1 for the approximate location of the Li and H atoms.) In fact, only at $N \approx 10$ does ρ begins to extend all around the molecule, although before this the helium density has already begun to form layers at the Li end of the molecule. Because of the very large zero-point motion of all degrees of freedom (^{4}He and LiH translation, LiH rotation), for these clusters it is meaningless to give specific values of N where the first "solvation shell" becomes complete. For $N = 20$, ^{4}He can be found all around LiH with a near uniform probability apart from the global minimum where it is markedly higher. As the size is further increased to $N = 40$, there is a faint demarcation between the density at the Li atom and the rest of the ^{4}He shell, with the otherwise almost uniform first solvation shell seeming to split into two "subshells" near the Li atom. As we approach $N = 100$, a third ^{4}He solvation layer has grown but the radial modulation of this is weak (and even weaker at the Li end). Furthermore, as N increases, the primary density peak near the Li atom widens toward the saddle joining the peak with the rest of the first solvation shell.

An exact specification of a well-defined peak region is therefore of course not possible. But a contructive and unambigous definition which can be applied to other cases of sharp density peaks as well is the following: we integrate $\rho(R,z)$ within an isosurface of constant density κ that defines a corresponding volume $\Delta V(\kappa)$

$$\Delta N(\kappa) = 2\pi \int_{\Delta V(\kappa)} \mathrm{d}z\, \mathrm{d}R\, R\rho(R,z) \qquad (1)$$

$\Delta N(\kappa)$ is thus the average number of particles in the region where $\rho(R,z)$ is greater than κ. As long as κ is above a threshold value κ_0, this region can be identified as a region enclosing the density peak. The values of $\Delta N(\kappa)$ as a function of κ are shown in Figure 6. The sharp upturn of $\Delta N(\kappa)$ at small κ values indicates that κ has dropped below the (N-dependent) threshold κ_0 here and $\Delta V(\kappa)$ now also comprises regions outside the main peak. Hence we can regard $\Delta N(\kappa_0)$ as a lower bound for the number of particles in the density peak. While Figure 6 shows that, just as is seen for $\rho(R, z)$, there is significant time step bias in $\Delta N(\kappa)$ (compare the dotted and solid lines for $N = 20$), we see that $\Delta N(\kappa_0)$ is nevertheless consistently close to unity for all N. Hence, if one accepts this constructive definition of the number of particles in the primary peak, we can conclude

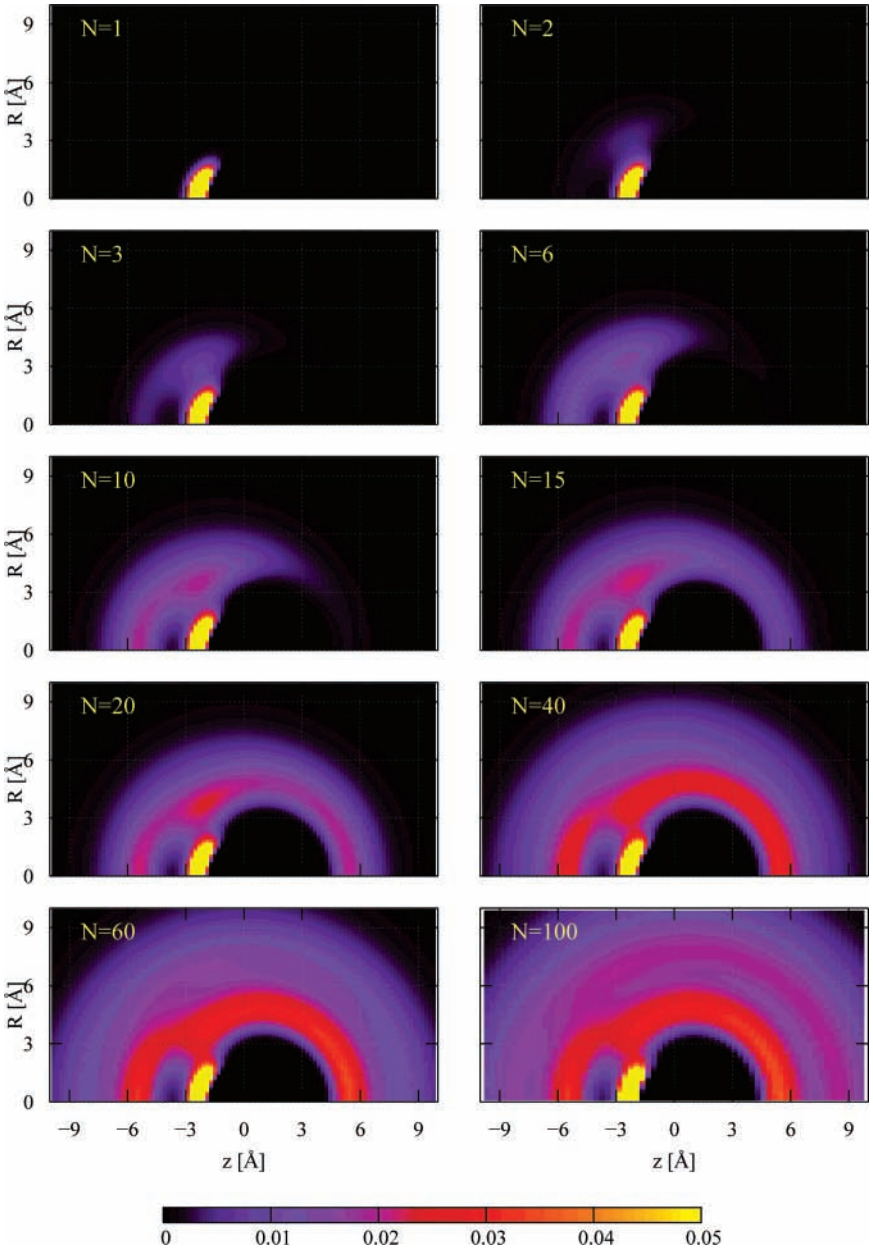

Figure 5. ^{4}He ground state densities $\rho(R, z)$ for the clusters LiH$-^4$He$_N$ plotted for several cluster sizes N as a function of R and z (see Figure 1 for definition of R and z and for the locations of Li and H). All simulations are made at $T = 0.3125$ K ($\beta = 3.2$ K^{-1}), using a time step of $\Delta\tau = 1/80$ K^{-1}. Note the region of lower density on the molecular axis lying between the high density (yellow) peak in the global minimum region and the rest of the first solvation shell (red band). The color scale shows the corresponding density scale in units of Å^{-3}.

that for all N the main density peak is made up of a single ^{4}He atom. We note that an estimate based on integrating $\rho(R, z)$ further out to the saddle region for larger N would significantly increase the estimate of the number of atoms in the peak to more than two, because of the R weight in the integral (1).

We have investigated the time step bias on the density $\rho(R, z)$ for $N = 20$, comparing the densities at time step values $\Delta\tau = 1/80$ K^{-1} and $\Delta\tau = 1/160$ K^{-1}. This comparison (not shown here) confirms what we have alleged above, namely that the time step bias is primarily important in the global minimum region while the density in other regions is less dependent on the value of $\Delta\tau$. Very close to LiH, where $\rho(R, z)$ becomes small, the time step bias of the density $\Delta\rho$ *relative* to the density ρ, $\Delta\rho/\rho$, is also large. This is easy to understand: the effective sizes of LiH and ^{4}He are larger than is suggested by the interaction potential, because of their large zero point motion. Larger time steps render the dynamics of the particles more classical, so that He and LiH can approach one another more closely, thus increasing the relative bias $\Delta\rho(R, z)/\rho(R, z)$. This strong time step bias in regions close to the molecule is also evident in Figure 3 where we see that as the time step $\Delta\tau$ is decreased, not only is the ^{4}He density peak smoothed out but also its average moves slightly further away from LiH.

The sharp peak of ρ at the global minimum indicates that helium is strongly bound there. This poses the question as to whether the He atoms sitting in this favored spot is forming a complex with LiH strong enough to suppress Bose permutation exchange with the other He atoms, as was seen with benzene[26] and larger aromatic molecules.[27] To address this question, we have analyzed the distributions of PIMC paths. The density of particles engaged in m-particle exchange, ρ_m, has no physical meaning per se, but it provides a qualitative indicator of local nonsuperfluid density and serves useful illustrative purposes. In particular, if $\rho_1 \approx \rho$ in the global mininum region, any He atom there could be considered to form a molecule-like complex with LiH that is solvated by the other He atoms. Figure 7, which

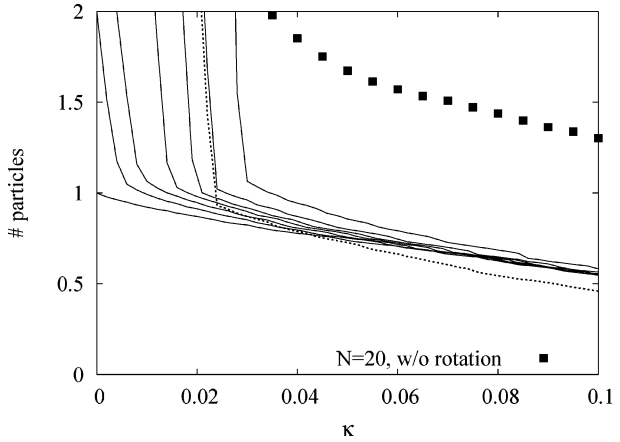

Figure 6. Integrated density $\Delta N = \int_{\Delta V} \rho(R,z)$, where ΔV is the volume enclosed by surface(s) of constant density κ, plotted as a function of κ for $N = 1, 2, 3, 6, 10, 20, 40$ (lines), where $\beta = 3.2$ K^{-1}. Higher values of ΔN correspond to larger N. The time step was $\Delta\tau = 1/80$ K^{-1}. For $N = 20$, we also show the result for $\Delta\tau = 1/160$ K^{-1} (dotted line). Also shown is ΔN for a hypothetical $N = 20$ cluster where the LiH rotation is switched off (filled squares).

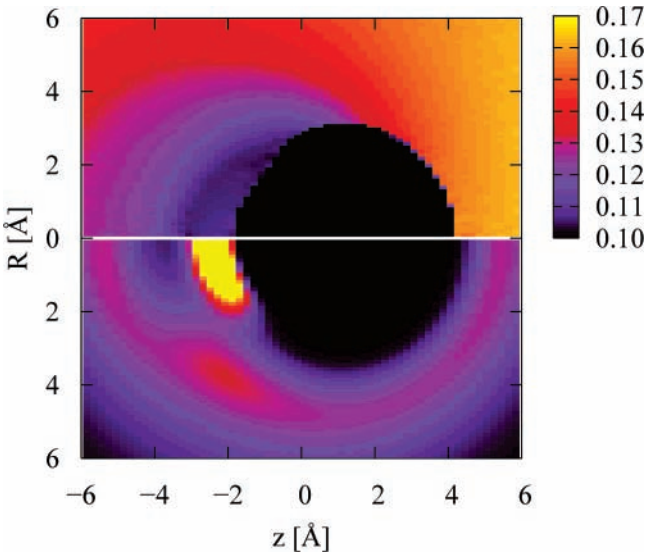

Figure 7. Top: relative density of nonexchanging ^{4}He paths, ρ_1/ρ, for LiH$-^4$He$_N$ clusters with $N = 20$ at $T = 0.3125$ K plotted as a function of R and z for calculations with $\Delta\tau = 1/160$ K^{-1} (the color scale for ρ_1/ρ is shown on the right). For reference, the full density ρ is shown below (the color scale for ρ is shown in Figure 5). Note that ρ_1/ρ is *lowest* where the density ρ is highest, i.e., at the density peak in the global potential minimum.

shows the density distribution of nonpermuting atoms, shows that this is not the case. In fact, the density of nonpermuting He atoms relative to the full density, ρ_1/ρ, is actually slightly *decreased* in this primary density peak, to a value of about 0.105 for $\Delta\tau = 1/160$ K^{-1}. Using also the result from $\Delta\tau = 1/80$ K^{-1} and assuming a linear extrapolation of ρ_1/ρ to zero time step, we estimate that $\rho_1/\rho \approx 0.115$ in the density peak, which is still lower than ρ_1/ρ in the rest of the solvation shell where the time step bias of ρ_1/ρ is insignificant. It appears that due to the large zero-point rotation of LiH in the effective potential of the helium environment, the Bose exchange of He atoms that sit in the global minimum is not hindered at all. Higher relative exchange densities ρ_m/ρ are even less dependent on the position (z, R) than ρ_1/ρ, thus confirming that Bose exchange is not suppressed in the density peak. This situation is very different from that observed previously in helium solvation of more strongly bound molecules where the helium permutations generally decrease in the neighborhood of the molecule, resulting in a local nonsuperfluid density.[2]

In order to assess the role of the large zero-point rotation of LiH, we perform PIMC simulations with the rotational degrees of freedom switched off (i.e., we set $B = 0$). Then the nonpermuting density fraction ρ_1/ρ in the global minimum region is indeed *increased*, indicating that the rotational motion of LiH enhances the permutations. However, we note that the whole ^{4}He solvation structure also changes profoundly when the rotation of LiH is removed: the main density peak of $\rho(R, z)$ is not located on the molecular axis anymore, but $\rho(R, z)$ peaks at finite R, indicating a "ring" surrounding the global minium. Figure 6 shows that this ring corresponds to roughly two ^{4}He atoms (filled squares).

The helium density in the molecular frame $\rho(R, z)$ does not provide unambigous information regarding the location of the LiH molecule in the cluster, namely whether LiH is solvated in the interior of the ^{4}He cluster or floats on its surface. To analyze this aspect of the structure, we calculate the LiH density with respect to the center of mass of the cluster, i.e., we calculated the probability density $\rho_{\mathrm{LiH}}(r)$ to find the center of mass of LiH a distance r away from the center of mass of the whole LiH$-^4$He $_N$ cluster. If LiH is fully solvated and sits at the center of the helium cluster, we expect $\rho_{\mathrm{LiH}}(r)$ to peak at $r = 0$. If, however, LiH floats on the surface of the cluster, we expect that $\rho_{\mathrm{LiH}}(r)$ will peak at a nonzero value $r > 0$ and that $\rho_{\mathrm{LiH}}(r)$ will go to zero at $r = 0$ as the cluster size N increases. Figure 8 shows $\rho_{\mathrm{LiH}}(r)$ for cluster sizes between $N = 6$ and $N = 100$ (the left panel shows the number density $\rho_{LiH}(r)$ and the right panel the probability density $r^2\rho_{\mathrm{LiH}}(r)$). For $N = 6$ and $N = 10$, LiH is clearly not sitting at the center of mass of the cluster. Between $N = 10$ and $N = 15$, LiH moves to the center and stays there as N is further increased up to the largest cluster we have simulated, $N = 100$. From $N = 20$ to $N = 100$ we can already observe a slight broading of the density distribution $\rho_{\mathrm{LiH}}(r)$ compared to that for the smaller clusters (see right panel). This is due to the weakening of the effective confinement potential provided by the cluster with increasing size.[28] From this analysis we can expect that LiH resides in the interior also for large droplets of thousands of helium atoms.

III. Excited States: Rotational Spectrum

Our primary interest in LiH$-^4$He$_N$ clusters concerns the rotational excitation spectrum. In principle, the excitation spectrum of a quantum many-body system can be calculated with the path integral correlation function (PICF) approach[22,23] where an imaginary time autocorrelation functions is sampled with PIMC. In the present case of rotational excitations of LiH in ^{4}He$_N$ clusters, the orientational autocorrelation function of the solvated molecule is sampled, i.e., $S(\tau) = \langle\Omega(\tau)\Omega(0)\rangle$, where Ω is the orientation vector of the linear molecule, $\tau \in [0,\beta[$ is the imaginary time, and the brackets $\langle\cdot\rangle$ denote the canonical ensemble average. Subsequently, $S(\tau)$ is numerically Laplace-inverted to the real frequency domain, $S(\tau) \rightarrow \tilde{S}(\omega)$, using the maximum entropy (MaxEnt) implementation of ref 29. This inversion is approximate and we refer to the spectrum thus obtained as the "MaxEnt spectrum". For example, owing to the smoothing property of the entropy term in the MaxEnt inversion procedure, the inverted spectrum is typically smoother than the real spectrum of molecular rotation in ^{4}He which all experimental evidence so far has shown to have narrow lines.[18] Therefore, in this section, we interpret a smooth peak in the MaxEnt spectrum as a single transition whose position and spectral weight coincide with the maximum of and integral over

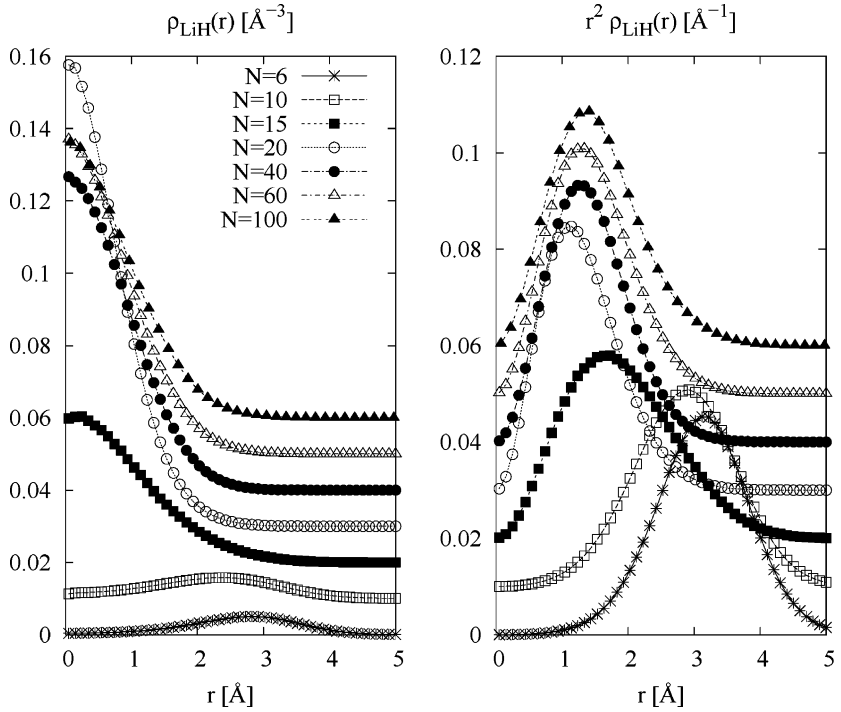

Figure 8. LiH ground state densities with respect to the LiH−^{4}He$_N$ cluster center of mass. $\rho_{LiH}(r)$ is normalized to unity, according to $\int d^3r\, \rho_{LiH}(r) = 4\pi \int dr\, r^2\rho_{LiH}(r) = 1$. The left panel shows the number density $\rho_{LiH}(r)$, for several cluster sizes N. The right panel shows the corresponding probability distributions $r^2\rho_{LiH}(r)$. All simulations were carried out at $T = 0.3125$ K ($\beta = 3.2$ K^{-1}), with a time step of $\Delta\tau = 1/80$ K^{-1}. Consecutive densities are offset for better visibility.

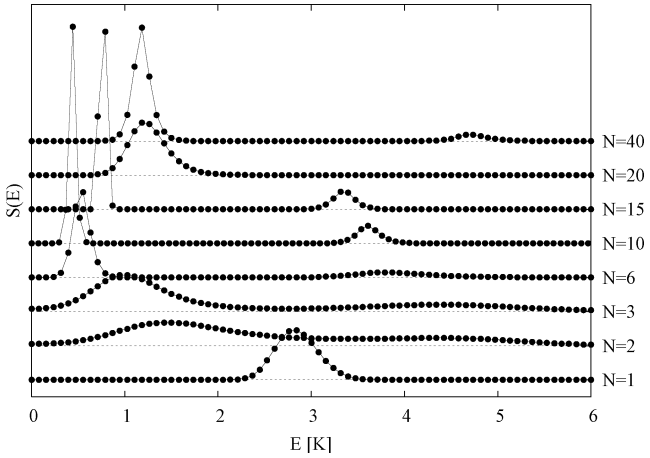

Figure 9. MaxEnt rotational spectra $S(E)$ of LiH in ^{4}He$_N$ clusters for several N (each spectrum offset for clarity) at $T = 0.3125$ K ($\beta = 3.2$ K^{-1}) for $N = 1;2;3;20;40$ and at $T = 0.156$ K ($\beta = 6.4$ K^{-1}) for $N = 6;10;15$, respectively, as explained in the text. All calculations were done with time step $\Delta\tau = 1/80$ K. For $N = 2$ and $N = 3$, the spectra are very broad, and have been scaled up by a factor of 2. Note that the line-shapes are smoothed by the MaxEnt Laplace inversion procedure, and we cannot extract spectral line widths.

the smooth MaxEnt peak, respectively. We show in section IV that merely fitting an effective free rotor correlation function[23,30] is not possible for LiH because this results in excessive violation of the exact sum rule $dS(\tau = 0)/d\tau = -2B$, where B is the *gas phase* rotational constant.[23]

In Figure 9, we show the $J = 1$ rotational MaxEnt spectra as a function of energy $E = \hbar\omega$, $S(E) \equiv \tilde{S}(\omega)$, for several cluster sizes N. We emphasize that the line shapes obtained by MaxEnt Laplace inversion of solvated molecule rotational spectra do not necessarily allow any conclusion about the physical line shape. For example, for $N = 1$ the true spectrum is a δ-function, while the corresponding line in the MaxEnt spectrum for $N = 1$ has nonzero width. For larger N, this leads of course to the question whether the broad MaxEnt lines may in fact be the envelope of several sharp lines. However, all experimental rotational spectra of molecule in ^{4}He until now have revealed only a single $J = 1$ transition (or at most two for small clusters, a-type and b-type, see below). Therefore, as mentioned above, in this section we will consider the smoothed peaks in the MaxEnt spectra as a single transition.

In addition to the primary peaks in Figure 9 which carry most of the spectral weights, we can discern weak secondary peaks (for $N = 2$, the primary and secondary peaks are so close that MaxEnt cannot fully resolve them, leading to overlapping peaks). Their energies are not statistically converged because of their low spectral weight, and we have not carried out further analysis of them. However, we note that for $N = 2 - 15$ these secondary peaks resemble the b-type transitions found in the rotational spectra of CO in ^{4}He clusters,[31] except that for LiH, the supposed b-type transition starts to appear for $N = 2$ rather than already for $N = 1$.[48] The end-over-end spectrum F_J for LiH in ^{4}He clusters (not shown here) corresponding to a-type transitions shows no such similarity with the corresponding spectrum for clusters containing CO. For CO, the primary peak of the end-over-end spectrum has a well-defined crossover with the rotational spectrum, i.e., with the b-type transitions.[23] For LiH, however, the end-over-end spectrum is, for all N, to a good approximation co-incident with the primary peak of the rotational spectrum. The coincidence of the molecule rotation and end-over-end spectrum indicates that the corresponding excitations are strongly coupled and consequently implies that a significant fraction of helium is following the LiH rotation. This situation is in strong contrast to that seen for CO, where we found that those two types of motion are not very strongly coupled at all, except in a crossover region at $N \sim 12$. For all N we also found weak spectral features at even higher energies, outside the energy range shown in Figure 9. Such high-energy features beyond the primary $J = 1$ peak in rotational spectra of

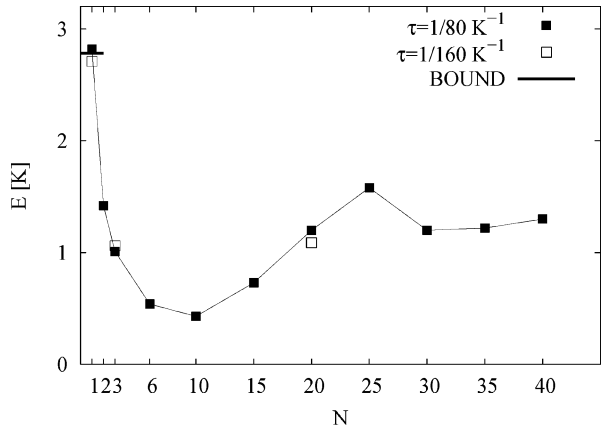

Figure 10. Rotational energies for $J = 1$ of LiH−^{4}He$_N$ (LiH in gas phase: $E_1 = 21.62$K) as a function of N. The filled boxes are for time step $\Delta\tau = 1/80$ K^{-1}, and the open boxes for $\Delta\tau = 1/160$ K^{-1}. The temperature is $T = 0.3125$ K except for $N = 6;10;15$ where $T = 0.156$ K. Also shown is the $J = 1$ excitation obtained with BOUND[25] for $N = 1$.

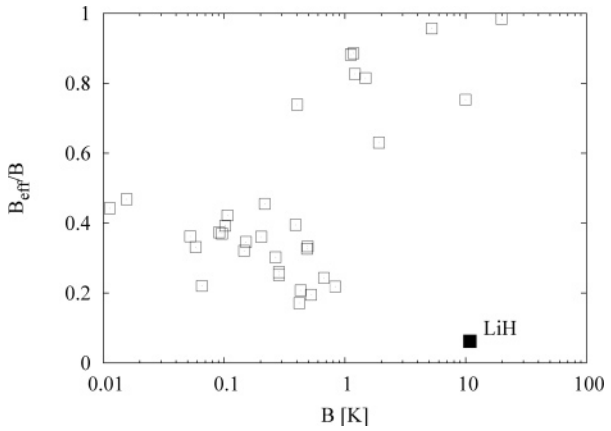

Figure 11. Comparison of the relative reduction B_{eff}/B of those molecules and complexes listed in Table 1 of ref 1 where the gas phase B is known (open boxes) with the calculated B_{eff}/B of LiH (filled box).

molecules solvated in ^{4}He must necessarily exist in order to fulfill exact sum rules.[23]

Figure 10 shows the main result of this work: the rotational energies E_J for $J = 1$ obtained from the MaxEnt spectra $S(E)$ as a function of cluster size N. The temperature is set to $T = 0.312$ K ($\beta = 3.2$ K^{-1}) for all N except for $N = 6;10;15$. For these sizes that correspond to the smallest observed B values, we choose a lower temperature, $T = 0.156$ K ($\beta = 6.4$ K^{-1}), in order to suppress the thermal population of rotational levels which would complicate the MaxEnt Laplace inversion. For $N = 1$, our PICF result compares favorably with the value of E_1 that was obtained with BOUND[25] (see section II). It is evident from Figure 10 that the relative reduction of B for LiH in helium is very large. We shall comment on this in some detail below. However, despite this unusually large reduction, we also observe the typical behavior found for all linear rotors in helium studied so far, namely that both experimentally and theoretically, for small N, the $J = 1$ rotational excitation energy E_1 falls with N, until at a size of the order of $N \approx 10$ there is a turnaround, and E_1 rises either to the large droplet/bulk limit or to a value lying still *above* that limit and showing an oscillatory behavior.[3,7,32−40] The latter situation is not yet fully understood. In the present case of LiH, we see an oscillation between $N = 20$ and $N = 25$, and then there is no significant change in E_1 between $N = 30$ and $N = 40$. However, $N = 40$ is still too small to be completely sure that we have reached the large droplet limit of E_1,[7] so we cannot rule out further changes of E_1 beyond $N = 40$ for LiH in ^{4}He$_N$.

All simulations were performed here with a time step of $\Delta\tau = 1/80$ K^{-1}. For $N = 1;3;20$ we have also performed simulations with $\Delta\tau = 1/160$ K^{-1}. The results are plotted in Figure 10 as open symbols. Comparison of results for two different time steps shows that the PICF excitation energies are less time step biased than ground state energies (Figure 4). We conclude that taking into account other uncertainties such as the LiH−He potential and the ill-conditioned nature of the inverse Laplace transformation, a time step of $\Delta\tau = 1/80$ K^{-1} is sufficiently small for the purpose of calculating rotational excitation energies.

The $J = 1$ rotational energy E_1 allows estimation of the effective linear rotational constant from the relation $E_1 = 2B_{\text{eff}}$, where we neglect the contribution of centrifugal distortion. For the largest cluster, $N = 40$, we obtain a value $B_{\text{eff}} = 0.66$ K. This results in a reduction relative to the gas phase B value of $B_{\text{eff}}/B = 0.0615$, i.e., the effective rotational constant is reduced to a mere 6% of the gas-phase value! A comparison of this reduction to that found experimentally for previously investigated molecules in large ^{4}He droplets is shown in Figure 11. While there is considerable scatter in the ratios B_{eff}/B, it is apparent that there is a clear trend toward a larger ratio for light molecules (i.e., B larger than about 1 K). LiH is therefore a remarkable exception lying far outside the regime of all other light molecules.

From the ground state results for energies and structure in section II, we recall that some ^{4}He density is strongly localized in the global minimum. The rotational motion of LiH and ^{4}He atoms in the global minimum is therefore likely to be highly correlated. This suggests a simple model for the rotational dynamics of LiH in the larger clusters, namely rotational motion of a core unit of LiH and one or more ^{4}He atoms. We consider here the smallest unit, namely a core dimer, with a single ^{4}He atom. First, we calculate the bare rotational energy of this dimer. The moment of inertia of the LiH−^{4}He dimer is determined from its ground state density (section II). Assuming this to be a rigid (prolate symmetric) top results in rotational constants $B = C = 2.1$ K, yielding a lowest $J = 1$ excitation energy of $E_1 = 4.2$ K. The actual value obtained from the MaxEnt inversion, $E_1 = 2.8$ K, is smaller because the dimer is very delocalized or "floppy" , but given that the model is rather crude, it is not surprising that it is 50% off. Now we can use this model of the dimer as a HeLiH "molecule" with "gas phase" rotational constant $B' = 2.8/2 = 1.4$ K as a reference point for the reduction of B' in larger clusters. With this dimer reference, we find that in the large N limit, the effective rotational constant B_{eff} with respect to this dimer "molecule" would be expected to be reduced by about 47%. Such a B_{eff}/B' ratio would be closer to the ratio of the molecules shown in Figure 11. Taking a larger core unit would only improve this estimate. Hence this simple model of a core rigidly bound unit appears to provide at least a qualitative understanding of the very large B_{eff} reduction with respect to the gas phase B for LiH in helium. We note that by introducing this dimer model (or models using a larger core unit) we do not want to imply that there is no exchange between ^{4}He atoms of the core unit and the other ^{4}He atoms; in fact we saw above that exchange is actually enhanced in the density peak region.

IV. Bose vs Boltzmann

One of the consequences of superfluidity is the lack of a Q-branch in all recorded rovibrational spectra of linear molecules in ^{4}He and hence the conservation of the linear rotor symmetry.

Another consequence is little dissipative molecule-matrix coupling, so that sharp spectral features are generally retained. Comparison with spectra obtained in ^{3}He, which obeys Fermi statistics, indicated that the bosonic nature of ^{4}He is responsible for this.[41,42]

In ref 43, the dynamic structure−function $S(k, \omega)$ of bulk ^{4}He was obtained with similar methods to those used here for molecule rotation spectra. A comparison there between ^{4}He obeying Bose and Boltzmann statistics, respectively, demonstrated the important role of Bose statistics for the spectrum of elementary excitations (phonon−roton spectrum). A key feature of $S(k, \omega)$ of bosonic ^{4}He below the superfluid transition temperature T_c, namely the energy gap below the elementary excitations, was reproduced qualitatively, while no such gap was present in "Boltzmann helium" .

In ref 23, we have found that the Bose statistics of the quantum solvent ^{4}He have a profound effect on the rotational dynamics of slow linear molecules like OCS when compared with corresponding results obtained with ^{4}He omitting permutation exchange. Unfortunately, for OCS, the effect could not be quantified in detail since statistical noise on the very small energy level spacing of such heavy molecules precluded MaxEnt inversion. In contrast, for the fast linear rotors HCCH[23] and CO,[44] we found surprisingly no significant effect of Bose statistics in the $J = 1$ MaxEnt spectrum.[23] In comparison to OCS, both of these molecules are light (fast) rotors with a solvation structure in ^{4}He that is much less anisotropic. A strongly bound heavy rotor such as OCS induces a strong anisotropic solvation structure in the surrounding helium that acts as a source of local excitations which give rise to a moment of inertia renormalization. While the ground states of Boltzmann and Bose helium are the same at zero temperature, both the local and collective excitations will be different in Bose and Boltzmann fluids. In the absence of analytical calculations of rotational spectra in Boltzmann helium, we cannot provide a definite explanation for the difference between OCS and the lighter molecules. However we note that it is not inconsistent with the current models for fast and slow rotors in superfluid helium. Thus, the rotational spectrum of HCCH and other light molecules with weakly anisotropic interactions with helium can be obtained by calculating the coupling to collective excitations:[5] apparently, this mechanism is little affected by the additional density of states in Boltzmann helium. On the other hand, slow molecules like OCS have a strongly anisotropic solvation structure in the surrounding helium, and the coupling between rotation and helium can be described well by a phenomenological two-fluid model.[2,40] The two-fluid model clearly relies on the predominantly superfluid state of helium around the molecule and hence is implicitly dependent on its Bose symmetry.

Now we ask the same question for the light molecule LiH solvated in ^{4}He, namely, does Bose symmetry affect the rotational dynamics of LiH? Given the light mass but strong anisotropy of its interaction with helium, the answer is not clear in advance. In Figure 12, we compare the orientational correlation function $S(\tau)$ of LiH solvated in a cluster ($N = 20$) of Bose and Boltzmann helium, respectively. For the Boltzmann case, $S(\tau)$ decays slower toward $\tau = \beta/2$, indicating the presence of excitations of lower energy. Hence, the situation for LiH is similar to the *slow* rotor OCS, and thus very different from the *fast* rotor HCCH (which, in the gas phase, is however still slow compared to LiH!). Unlike for OCS, statistical noise in the present case is small enough (smaller than symbol size in Figure 12) to allow MaxEnt inversion to obtain $S(E)$. This spectrum is

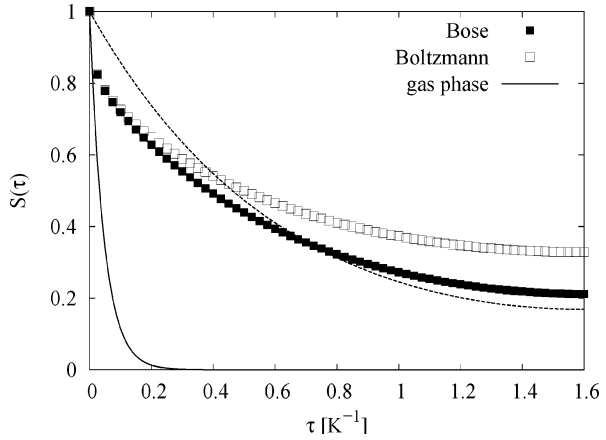

Figure 12. Orientational correlation function $S(\tau)$ sampled with PIMC is shown (points) for LiH−^{4}He$_N$, $N = 20$, at $T = 0.3125$ K for Bose ^{4}He (filled squares) and Boltzmann ^{4}He (open squares). $S(\tau)$ is shown for every other time step for better readability. The full line shows $S(\tau)$ for LiH in gas phase (the dashed line is $S(\tau)$ with fit parameter $B = B_{\text{eff}}$, which fits the data badly).

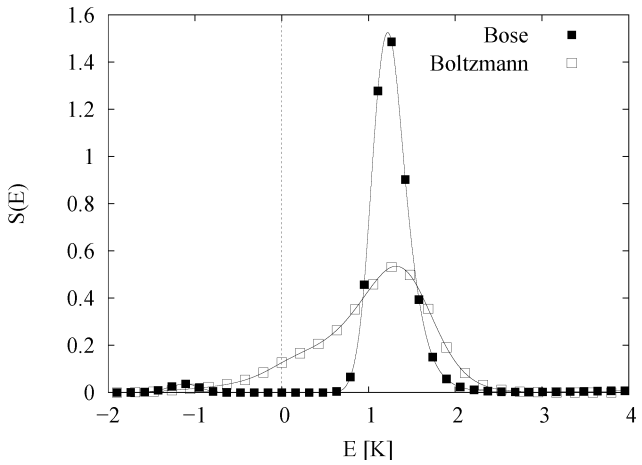

Figure 13. MaxEnt rotational spectrum $S(E)$ of LiH−^{4}He$_N$ for $N = 20$ at $T = 0.3125$ K ($\beta = 3.2$ K^{-1}), calculated assuming Bose statistics (filled squares) and Boltzmann statistics (open squares), respectively. The lines connecting the symbols are spline interpolations, made to guide the eye.

shown in Figure 13, where we now also show the corresponding peak in the negative energy range which is calculated using detailed balance, $S(-E) = e^{-\beta E/\hbar} S(E)$, and which corresponds to deexcitation of thermally populated excitations. For the Bose case, in the energy range shown in Figure 13, there is a narrow peak at 1.22 K carrying most of the spectral weight (78%, considering only the positive energy range). As mentioned above, we assume that this is a single sharp line, consistent with the experimental findings for many molecules, and we assign it to the R(0) transition of the solvated LiH, with its width of about 0.5 K constituting an approximate measure of the amount of artificial smoothing that the MaxEnt inversion introduces for this particular spectrum.[23] Correspondingly, the smaller deexcitation peak at −1.22 K with the same width is assigned to the P(1) transition.

The MaxEnt spectrum of LiH in Boltzmann helium in Figure 13 (open squares) peaks at a similar energy (1.32 K, spectral weight 77%), but is significantly broader. In particular at zero energy it lacks the "energy gap" seen in the Bose case. Therefore, while we cannot completely rule out that the Boltzmann example is a pathological case of excessive smoothing of a single sharp line due to MaxEnt, it is more likely that

the true spectrum consists of several sharp lines and that the smoothing characteristics of MaxEnt result here in an approximate continuous envelope of these lines. (Note that for a small cluster like $N = 20$, the spectrum cannot be smooth, but must be discrete for energies below the evaporation threshold, i.e., the chemical potential, of the droplet.) The MaxEnt spectrum is too broad to see individual peaks but its general shape is consistent with the presence of negative energy peaks corresponding to deexcitation. Hence, we believe that the following interpretation is correct: the true rotation spectrum of LiH in a small ($N = 20$) Bose cluster has an isolated, sharp R(0) line, while the spectrum in a small Boltzmann cluster consists of many lines with a broad envelope that has no energy gap.

An energy gap in the ^{4}He excitations for finite k is associated with superfluidity.[45] Here we have a similar situation, but it is the gap in the rotation spectrum of the *solute* that identifies the superfluidity of the *solvent*. Although there is a lot of indirect theoretical evidence for the role of superfluidity for sharp rotational spectra using, for example, the two-fluid approach for ^{4}He and the assumption of adiabatic following of the normal fraction to calculate and compare rotational constants with experimental values,[3,4] or from calculations of the local superfluid density,[37,46] we have here for the first time obtained direct theoretical evidence of how Bose permutation symmetry of the quantum solvent affects the rotational spectrum.

V. Conclusion

We have investigated small to medium sized LiH$-^4$He$_N$ clusters using PIMC simulations to obtain the solvation energy and structure as well as the rotational excitation spectra. Our results show that the LiH molecule is solvated in the center of the cluster (defined with respect to the total center of mass) for sizes $N > 10 - 15$, and that this solvated structure prevails up to the largest cluster simulated here, $N = 100$. We conjecture that LiH is solvated inside large ^{4}He droplets, despite its low mass (large zero-point motion) and despite the repulsion between He and the hydrogen end of LiH. Because of the anisotropic LiH$-$He interaction, the solvation structure is very anisotropic as well, with a distinct density peak in the global potential minimum. The solvation energy of He atoms for $N \geq 2$ is much smaller than the dimer binding energy, which can be seen in the N dependence of the chemical potential. Nevertheless, an analysis of the exchange path lengths show that the He atoms in the global minimum region are not classically localized "dead" atoms and still participate in permutation exchange with other He atoms. In fact, the permutation exchange propensity appears to be enhanced in this region, unlike the situation for more strongly bound molecules where it generally decreases near the global minimum region.

For calculation of the rotational spectrum, we used the path integral correlation function approach which has been successfully applied to the rotational spectra of other molecules solvated in ^{4}He.[23,38] For the N dependence of the rotational energies $2B_{\text{eff}}$ we found a similar shape for LiH as for other molecules, i.e., an initial drop of B_{eff}, followed by recovery and oscillation toward a limiting value. Unfortunately, there are as of the present time, no experimental data for B_{eff} of LiH in ^{4}He droplets that would allow independent determination of the limiting value. The scale of this calculated reduction in B_{eff} is vastly different from that observed for previously investigated molecules. For $N \gtrsim 20$, we found that B_{eff} is reduced to only about 6% of the gas-phase rotational constant. LiH thus not only deviates from all other light molecules in this respect, but furthermore appears to have the lowest ratio B_{eff}/B of all molecules which have been investigated up to now. This exceptional behavior is due to the strong anisotropy of the LiH$-$He interaction compared to other light molecules. A simple model which assumes that a core unit of one or more ^{4}He atoms bound in the global minimum moves adiabatically with the molecule but still participates in permutation exchanges provides a qualitative explanation of the large reduction.

We have also considered the artificial system of LiH solvated in a cluster of ^{4}He which obeys Boltzmann statistics instead of Bose statistics. Unlike the previously studied molecule OCS where the statistical noise was too high to obtain the rotational spectrum by MaxEnt, and also unlike the case of light molecules HCCH and CO, which induce relatively weak perturbations of the helium density and show no difference between the two statistics, we could show explicitly for LiH the existence of a marked difference between the rotational spectra in Bose and in Boltzmann helium. In this case we demonstrated that only in Bose helium is there a well-defined rotational line. In Boltzmann helium, the rotational spectrum (or, more precisely, its envelope) is much broader and does not vanish at zero energy, i.e., it has no low energy "gap". Comparison with the corresponding results for OCS, HCCH and CO respectively, indicates that in addition to high quality sampling statistics for the correlation functions, a very pronounced anisotropy of the helium density around the molecule is required to observe a dependence of the rotational spectrum on exchange statistics (Bose and Boltzmann).

On the technical side, a detailed study of the dimer, $N = 1$, showed that due to the steep global potential minimum, the PIMC time step bias is quite severe for the ground state energy. An accurate value for the ground state energies of LiH$-^4$He clusters may be obtained from values at time steps $\Delta\tau \leq 1/160$ K^{-1} by extrapolation to $\Delta\tau = 0$. The ground state distribution of ^{4}He around LiH changed little below $\Delta\tau = 1/160$ K^{-1} even for the peak in the global potential miminum. Since we are interested in the buildup of density around LiH as N is increased which is less affected by bias than this density peak, we found $\Delta\tau = 1/80$ K^{-1} to be sufficient for this purpose, and refrained from extrapolation to $\Delta\tau = 0$. For the excitation energies we found surprisingly little time step bias; therefore, extrapolation is not needed either. Nevertheless, our simulations show that the primitive approximation, as the name implies, is not the best choice for the density matrix, and a better approximation should be employed for strong solute$-$solvent interactions. A combination of the pair density matrix approximation for the spherical solvent$-$solvent interaction with a fourth-order scheme[24,47] for the anisotropic solute$-$solvent interaction can lead to significant reduction of the time-step bias on the energy. The applicability and benefits of such higher order propagators for molecules in quantum solvents will be discussed elsewhere.

Acknowledgment. We thank Brian K. Taylor for providing the LiH$-$He potential, and Yongkyung Kwon, Klaus von Haeften, and Francesco Paesani for helpful discussions. This work was supported by the Miller Institute for Basic Research in Science, the Fraunhofer Fellowship, and the ZID at the Kepler University, Linz, Austria, providing computational resources.

References and Notes

(1) Callegari, C.; Lehmann, K. K.; Schmied, R.; Scoles, G. *J. Chem. Phys.* **2001,** *115,* 10090.

(2) Kwon, Y.; Whaley, K. B. *Phys. Rev. Lett.* **1999,** *83,* 4108.

(3) Topic, W.; Jäger, W. J.; Blinov, N.; Roy, P.-N.; Botti, M.; Moroni, S. *J. Chem. Phys.* **2006,** *125,* 144310.

(4) Kwon, Y.; Huang, P.; Patel, M. V.; Blume, D.; Whaley, K. B. *J. Chem. Phys.* **2000,** *113*, 6469. Patel, M. V.; Viel, A.; Paesani, F.; Huang, P.; Whaley, K. B. *J. Chem. Phys.* **2003**, *118*, 5011−5027.
(5) Zillich, R.; Whaley, K. B. *Phys. Rev. B* **2004,** *6*, 104517.
(6) Zillich, R.; Kwon, Y.; Whaley, K. B. *Phys. Rev. Lett.* **2004,** *93*, 250401.
(7) van Haeften, K.; Rudolph, S.; Simanovski, I.; Havenith, M.; Zillich, R. E.; Whaley, K. B. *Phys. Rev. B* **2006,** *73*, 054502.
(8) Herzberg, G. *Molecular Spectra and Molecular Structure: Spectra of Diatomic Molecules*; Krieger: Melbourne, FL, 1989.
(9) Taylor, B. K.; Hinde, R. J. *J. Chem. Phys.* **1999,** *111*, 973.
(10) Taylor, B. K.; Hinde, R. J. *J. Chem. Phys.* **2005,** *112*, 074308.
(11) Barnett, R. N.; Whaley, K. B. *J. Chem. Phys.* **1992,** *96*, 2953.
(12) Nauta,K.; Miller, R. E. *Phys. Rev. Lett.* **1999,** *82*, 4480.
(13) Conjusteau, A.; Callegari, C.; Reinhard, I.; Lehmann, K. K.; Scoles, G. *J. Chem. Phys.* **2000,** *113*, 4840.
(14) Nauta, K.; Miller, R. E. *J. Chem. Phys.* **2001,** *115*, 8384.
(15) Nauta, K.; Miller, R. E. *J. Chem. Phys.* **2000,** *113*, 9466.
(16) Grebenev, S.; Hartmann, M.; Havenith, M.; Sartakov, B.; Toennies, J. P.; Vilesov, A. F. *J. Chem. Phys.* **2000,** *112*, 4485.
(17) Nauta, K.; Miller, R. E. *J. Chem. Phys.* **2001,** *115*, 10254.
(18) Toennies, J. P.; Vilesov, A. F. *Angew. Chem. Int. Ed.* **2004,** *43*, 2622.
(19) Miller, R. E. *Faraday Discuss.* **2001,** *118*, 1.
(20) Paesani, F. Unpublished.
(21) Williams, J.; Rohrbacher, A.; Djahandideh, D.; Janda, K. C.; Jamak, A.; Tao, F.-M.; Halberstadt, N. *Mol. Phys.* **1997,** *91*, 573.
(22) Ceperley, D. M. *Rev. Mod. Phys.* **1995,** *67*, 279.
(23) Zillich, R. E.; Paesani, F.; Kwon, Y.; Whaley, K. B. *J. Chem. Phys.* **2005,** *123*, 114301.
(24) Takahashi, M.; Imada, M. *J. Phys. Soc. Jpn.* **1984,** *53*, 3765.
(25) Hutson, J. M. *Bound computer code, version 5*, distributed by Collaborative Computational Project No. 6 of the Science and Engineering Research Council (U.K.), 1993.
(26) Kwon, Y.; Whaley, K. B. *Phys. Rev. Lett.* **2002,** *89*, 273401.
(27) Whitley, H.; Huang, P.; Kwon, Y.; Whaley, K. B. *J. Chem. Phys.* **2005,** *123*, 054807.
(28) Lehmann, K. K. *Mol. Phys.* **1999,** *97*, 645.
(29) Bryan, R. K. *Eur. Biophys. J.* **1990,** *18*, 165.
(30) Blinov, N.; Song, X.; Roy, P. *J. Chem. Phys.* **2004,** *120*, 5916.
(31) Tang, J.; McKellar, A. R. W. *J. Chem. Phys.* **2003,** *119*, 754.
(32) Paesani, F.; Viel, A.; Gianturco, F. A.; Whaley, K. B. *Phys. Rev. Lett.* **2003,** *90*, 073401.
(33) Xu, Y.; Jäger, W.; Tang, J.; McKellar, A. R. W. *Phys. Rev. Lett.* **2003,** *191*, 163401.
(34) Tang, J.; McKellar, A.; Mezzacapo, F.; Moroni, S. *Phys. Rev. Lett.* **2004,** *92*, 145503.
(35) Moroni, S.; Blinov, N.; Roy, P.-N. *J. Chem. Phys.* **2004,** *121*, 3577.
(36) Paesani, F.; Whaley, K. B. *J. Chem. Phys.* **2004,** *121*, 5293.
(37) Paesani, F.; Kwon, Y.; Whaley, K. B. *Phys. Rev. Lett.* **2005,** *94*, 153401.
(38) Blinov, N.; Roy, P.-N. *J. Low Temp. Phys.* **2005,** *140*, 253.
(39) McKellar, A. R. W.; Xu, Y.; Jäger, W. *Phys. Rev. Lett.* **2006,** *97*, 183401.
(40) Xu, Y.; Blinov, N.; Jäger, W.; Roy, P.-N. *J. Chem. Phys.* **2006,** *124*, 081101.
(41) Grebenev, S.; Toennies, J. P.; Vilesov, A. F. *Science* **1998,** *279*, 2083.
(42) Babichenko, V. S.; Kagan, Y. *Phys. Rev. Lett.* **1999,** *83*, 3458.
(43) Boninsegni, M.; Ceperley, D. M.; of Low, J. *Temp. Phys.* **1996,** *104*, 339.
(44) Zillich, R. E. Unpublished work.
(45) Tilley, D. R.; Tilley, J. *Superfluidity and Superconductivity*; Hilger: Bristol, U.K., 1986).
(46) Kwon, Y.; Paesani, F.; Whaley, K. B. *Phys. Rev. B* **2006,** *74*, 174522.
(47) Chin, S. A.; Chen, C. R. *J. Chem. Phys.* **2002,** *117*, 1409.
(48) This notation refers to a molecule−He dimer, where b-type transitions correspond to molecular rotations, and a-type transitions to end-over-end motion of the He relative to the molecule. In clusters, for a given total angular momentum J, the molecular rotations can be accessed by the molecular correlation function $S_J(\tau)$ and the end-over-end motion by a correlation function of collective helium coordinates, $F_J(\tau) = \sum_m \sum_{i,j} \langle Y^*_{Jm}(\Omega_i(\tau)) Y_{Jm}(\Omega_j(\tau)) \rangle$ where Ω_i is the orientation of atom i relative to the molecule.[23]